Dispersion of Electromagnetic Waves in a Periodic Open Waveguide

Master Thesis

to be defended publicly
on Tuesday 09 March 2010 at 1.30 pm
by

Capt K.J. Potman

Captain, Royal Netherlands Air Force
Delft University of Technology
Delft, The Netherlands

koen.potman@gmail.com
student # 1282433

15 April 2010

This graduation work has been carried out at the Laboratory of Electromagnetic Research of the Delft University of Technology

The Royal Netherlands Air Force (RNLAF) financially supported this work.

Committee members

Prof.dr. T.D. Visser	Delft University of Technology, EEMCS, Chair
Dr.ir. M.D. Verweij	Delft University of Technology, EEMCS Supervisor
Dr.ir. S. van den Berg	Thales Netherlands
Dr. K.W.A. van Dongen	Delft University of Technology, AS

An electronic copy in Portable Document Format (PDF) of this work can be found at sites.google.com/site/koenpotman/downloads

Preface

This report is the final thesis to obtain my M.Sc. degree in Electrical Engineering at Delft University of Technology. In the last eight months I have mastered the topic of periodic open waveguides in general and surface waves in such structures specifically.

The research, performed at the Laboratory of Electromagnetic Research, focused on the analysis of a two-dimensional periodic open waveguide using a new method without making any assumptions about the size of the slots with respect to the spatial period. This work would not have been accomplished with the help of a number of people.

First of all I would like to thank dr.ir. M.D. Verweij, who has been my daily supervisor. Thank you for always asking the critical questions when I was enthusiast about (intermediate) results and for motivating me when necessary. Your way of supervision, giving me freedom when possible and taking control when needed, I have experienced as very pleasant.

Next, I wish to thank my parents and parents-in-law for showing so much interest, supporting me when necessary and for the numerous times they have taken care of their grandchildren when 'daddy' was busy studying.

This thesis, I dedicate to Liesbeth, my consort. Thank you so much for giving me the opportunity to face this intellectual challenge, all the support and all the love you have given me.

Koen Potman
Apeldoorn, 21.02.2010

Abstract

Phased array antennas are found in many variations. The two main advantages of phased array antennas are their compactness and their ability to perform high speed beam steering. This makes them very useful for mobile systems like the Patriot missile system of the RNLAF.

In one way or the other a phased array antenna is to be considered as a periodic structure, either periodically placed separate radiating elements or some kind of slotted waveguide. It is not unusual that these antennas are covered with a metallic structure that is mechanically supported by a dielectric layer. Such structures enable the appearance of surface waves to travel along the structure.

In some applications these surface waves are a desired phenomenon, in other they are not. When undesired, these surface waves, also known as guided or propagating modes, cause a loss of energy and possibly returns from unwanted directions.

In this report we model the guided modes for an infinitely long structure in the lateral direction, that is invariant in the transverse direction. This modeling is done without making any assumptions about the width of the slots relative to the spatial period. We do this by representing the electric field by their Floquet series in combination with a plane wave representation for the field between the plates. Applying the appropriate boundary conditions leads us to a determinantal (or dispersion) equation.

Complex solutions to this dispersion equation have been found numerically using a sophisticatedly adjusted downhill method in two dimensions. Finally this new method has been used to show the effect of the variation of four important parameters in the modeling of a periodically loaded open waveguide. These parameters are: the number of space harmonics, the permittivity of the dielectric layer, the slot size and the height of the dielectric layer.

Contents

Chapter One

Introduction

1.1 Introduction to periodic structures

The first study of (mechanical) periodic lattices was performed by Isaac Newton and dates back to the end of the seventeenth century. In the eighteenth century the work was continued by father and son Bernoulli. Also Taylor, Fourier, Euler and Lagrange worked on problems related to (1-D) periodic lattices. In 1830, it was Cauchy who used Newton's mechanical model in an attempt to find a model for the dispersion of optical waves [8]. During the second World War scientific research in the area of electromagnetic radiation, scattering and imaging, including periodic open waveguides, flew a high pitch, although, for obvious reasons, not much was published during this period.

In the beginning of the '60 of the previous century it was, amongst others, A.A. Oliner who focused research on periodic modulated slow wave structures. In his paper [17] Oliner has identified several periodically-modulated slow-wave structures amongst which a strip-loaded-dielectric slab. R.A. Sigelmann has used two methods in his paper [20] to obtain the surface-wave modes, when a field is generated by a magnetic line current in such a structure. A very thorough investigation on periodically-modulated slow-wave structures has been performed by Jacobsen [15]. This paper focuses on modulation of the E-field (by covering a dielectric slab with narrow strips) and makes use of the so-called Hertzian potentials. Balling focused his master-of-science thesis (supervised by Jacobsen) and the resulting publication [6] on similar structures, but now covered in wide strips.

More recently, Yariv, Yeh and Hong [23] describe a general theory of electromagnetic propagation in periodic media using the theory of Bloch modes, forbidden gaps, evanescent waves and surface waves. The scattering of electromagnetic waves from a dielectric slab loaded with a periodic array of perfectly conducting strips has been analyzed by Kalhor [16].

In periodic structures the electromagnetic field will only contain waves with a periodicity related to that of the structure, i.e. it can be described as a plane wave expansion (so called space harmonics) times a function with a periodicity related to that of the structure. These plane waves are called Bloch (or Floquet) waves or Bloch (or Floquet) modes. The phenomenon of a Bloch state was developed by Felix Bloch in 1928. It describes the conduction of electrons in crystalline solids. The same concept (with its mathematics) was also discovered independently by George William Hill (1877), Gaston Floquet (1883), and Alexander Lyapunov (1892). This has led to a variety of nomenclatures. As common in the used literature, in this work we will apply the theorem to our partial differential equations and use the term "Floquet theorem".

The analysis of the propagation characteristics of the aforementioned plane waves in a general 1-D periodic structure, can be done best by using a dispersion diagram. A quantification for the fundamental field quantity for TE-fields can be found by using a plane wave expansion, whichs leads to a (semi) infinite matrix-vector equation. A dispersion equation is found by letting the determinant of the system matrix vanish.

1.2 Application of periodic open structures

The application of periodic open structures is found in the area of Travelling Wave Antennas (TWA). TWA are wave guiding structures that radiate from one or more points in the (periodic open) aperture. Usually TWA's are fed from a single source. Effective use of travelling wave structures as antenna requires detailed knowledge of the propagation characteristics of the structure. Three different types of TWA's can be distinguished: leaky-wave antennas (LWA), surface-wave antennas and log-periodic antennas [19]. In these cases surface waves are intentionally generated and used to transport electromagnetic energy. However, in some cases surface waves can appear unintentionally.

1.3 Surface waves guiding structures

Open waveguides capable of guiding surfaces waves can be classified in different ways. One often used, is to make a distinction between periodic and non-periodic structures (as done in [24]). Periodic structures can be

divided into structures with continuous periodically varying electrical properties and structures with periodic boundary conditions [11]. Waveguides of the latter type are shown in sub-figures b,d,e,g and h of figure 1.1. The other (non-periodic) waveguides are said to have a smooth interface. "Leaky waveguides" refer to shielded waveguides that are coupled to space through one or several slots through which (for certain frequencies) energy can leak away from the waveguide. Leaky waveguides can be placed between open and closed waveguides.

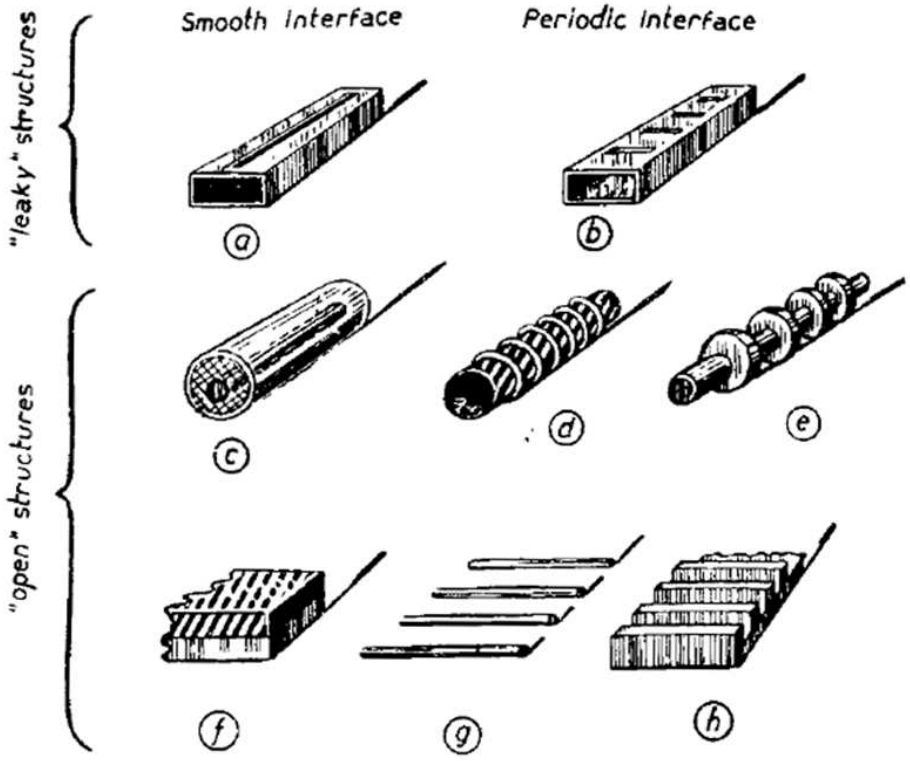

Figure 1.1: waveguide structures (from [24])

1.4 This report

In this report we answer the question for which frequencies surface waves appear on a periodic structure. That is, to find which modes may propagate in the lateral direction (relative to the normal on the array). To do this, we have developed a new method for the derivation of the dispersion relation for periodic open structures, using a plane wave expansion. We do not make any assumptions about the strips loading the structure being narrow or wide as

done by e.g. Jacobsen and Balling. This report is organised in the following manner. Chapter 2 introduces the configuration studied, the basic equations and the boundary conditions. Floquet's theorem is explained followed by our numerical method. In chapter 3 the results of our method are shown. In chapter 4, the final chapter, we present our conclusions according to the method we have described in chapter 3 and discuss the possible subsequent research.

Chapter Two

Theory

2.1 Introduction

As a defence contractor Thales is using array antenna technology in a diversity of applications. An antenna array is a combination of single antenna elements in an array. One specific configuration used, is described in the following paragraph. For this configuration, at certain frequencies surface waves are travelling in the lateral direction (parallel to the plates). There are several reasons why these lateral waves are undesirable. Foremost they cause a loss of energy and may cause all sorts of echoes from unwanted directions. However, before answering the question of why surface waves appear the question of what surface waves are, should be answered.

Surface waves are also known as Zenneck waves, named after their discoverer Zenneck. Surface waves exist at the interface of two media and are a solution to the Maxwell's equations for a specific problem. Sometimes a comparison to waves on a water surface is made. This, however, is *misleading*. Water waves only exist at the air-water boundary itself, while in our case surface waves also manifest themselves in the neighborhood of the boundary. The boundary is used to guide the waves. Surface waves are a class of guided waves.

2.2 Configuration

A common configuration used by Thales is a dielectric on which metal patches are placed. In analysis, progress is best made by dividing the problem in smaller and generally simpler subproblems. We, as a first step, consider a two dimensional configuration that is invariant in the x_2-direction. A (right-handed) Cartesian reference frame is introduced and the period (d), the hole-size (a) and the thickness of the dielectric (h) are defined as in figure 2.1. The dielectric rests on a perfectly conducting plate and is covered

by perfectly conducting strips. Thereby two regions are defined.

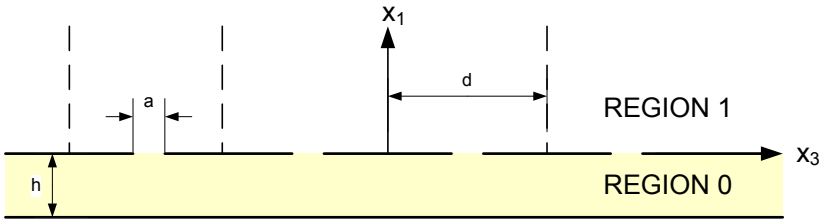

Figure 2.1: Definition of the periodic structure

2.3 Dispersion diagrams

Before starting modelling electromagnetic waves in a periodic structure, we will have a closer look at dispersion diagrams. Dispersion is the phenomenon in which the propagation coefficient of a wave depends on its frequency. A dispersion diagram shows this relation.

Often such a diagram is split in two parts. Figure 2.2 (from [19]) shows the real part β of the propagation coefficient k_{30} versus ω. We will later also have a look at the imaginary part α. The multiplication of the x-axis by d and the y-axis by $\sqrt{\epsilon_0\mu_0}d$, as $k_0 = \omega\sqrt{\epsilon_0\mu_0}$, is a result of the normalisation described in appendix C.

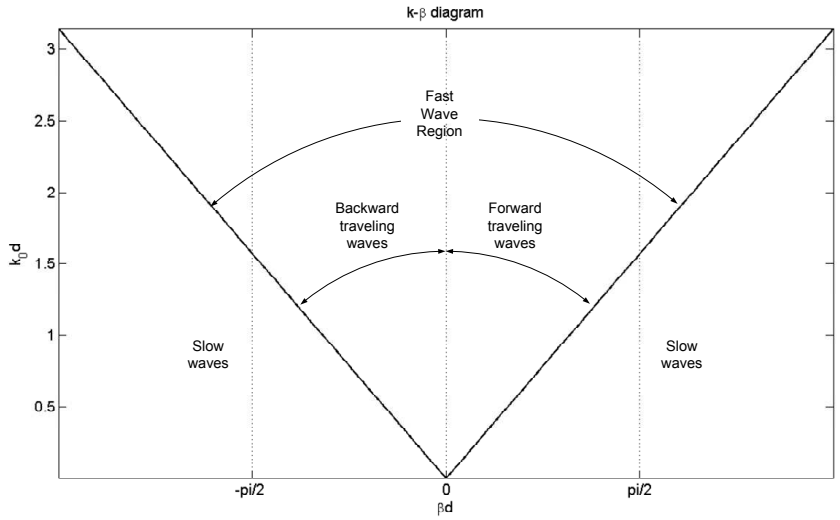

Figure 2.2: Different regions in the $k_0 - \beta$ plane

As shown in figure 2.2 a dispersion plot can be divided in four different regions. The area left of the line $\beta d = 0$ corresponds to backward travelling waves. The area to the right corresponds to forward travelling waves. The line $k_0 = \pm\beta$ corresponds to waves travelling with free space velocity along the structure, either for- or backward. For the slope of this line in figure 2.2 we have:

$$\frac{k_0}{k_{30}} = 1 \tag{2.1}$$

using the relation $k_0 = \omega\sqrt{\epsilon_0\mu_0}$, we can write

$$k_0 = \frac{\omega}{c_0} = k_{30} \tag{2.2}$$

For higher slopes this implies:

$$k = \frac{\omega}{c} = \frac{\omega}{bc_0} = k_{30}; \qquad b > 1 \tag{2.3}$$

Thus both areas are divided in a fast wave region (FWR) ($c > c_0$), and a region for slow waves where $c < c_0$.

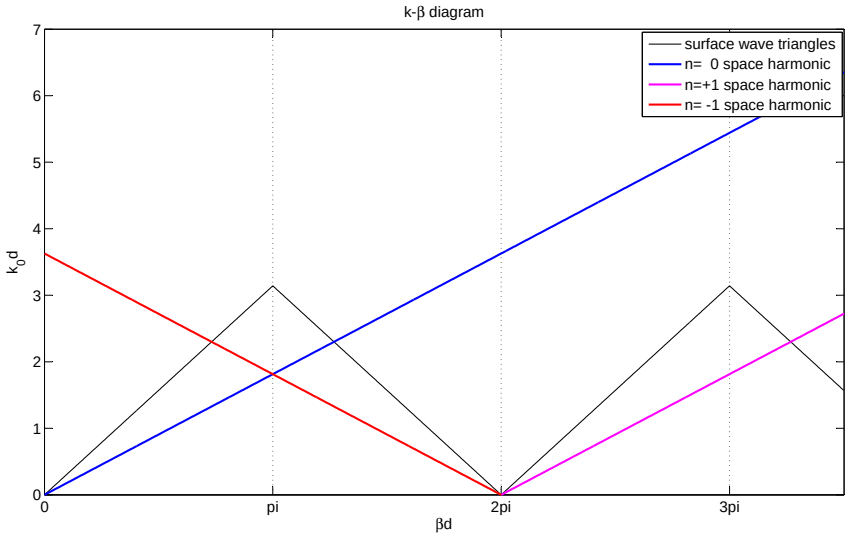

Figure 2.3: Dispersion plot for a periodic basically slow travelling-wave structure for vanishing loading [19]

From [19] we know that the dispersion relation of a basically slow open travelling wave structure with vanishing loading is given by $\beta^2 - \epsilon k_0^2 = 0$. Its graphical representation is shown in figure 2.3. Increasing the permittivity

of the waveguide decreases the wavespeed and thus the angle of the dispersion curve.

A basically slow loaded travelling waveguide is a waveguide that supports a wave with phase velocity c_{ph} slower than light ($c_{ph} < c_0$), when the loading is removed. Two other classes of loaded travelling waveguides are the basically TEM ($c_{ph} = c_0$) and the basically fast ($c_{ph} > c_0$) loaded travelling waveguides, examples of each type can be found in [19]. For sufficiently low frequencies ($d < \frac{\lambda_0}{2}$) the former two TWA's support a surface wave. When the frequency is raised the surface wave antenna turns into a frequency scanned (leaky wave) antenna.

For periodic structures the overall $k_0 d - \beta d$ plot can be considered as a superposition of multiple $k_0 d - \beta d$ plots, one for each cell. Given n cells, this leads to n different fast wave regions, shifted over a period of 2π. Combining all the individual $k_0 d - \beta d$ plots leads to the triangles as shown in figure 2.3. As is clear not only the FWR is repeated every 2π. The dispersion curves are repeated with the same period. Now, if one of these dispersion curves enters the basic FWR (that is the region around the $k_0 d$-axis), this means that the guided mode of the corresponding space harmonic turns into a radiating mode.

Looking at figure 2.3 we notice that the dispersion curve of the basic ($n = 0$) space harmonic and that of the first backward ($n = -1$) space harmonic intersect. At this point the so called mode-coupling effect occurs and it corresponds to the location of a (close-waveguide type) stopband. Mode-coupling for the basic ($n = 0$) and $n = -1$ space harmonic means that they have the same propagation coefficient $k_{30} = \pi$, resulting in a standing wave. A standing wave means no propagation of electromagnetic waves, which is interpreted as a stopband.

Table 2.1: coupling regions in the $k - \beta$ diagram [15]

region	**behaviour**
before 1	no propagation
1 - 2	propagation, no attenuation, purely bound surface wave
2 - 3	stopband, closed waveguide standing wave type behaviour
3 - 4	propagation, no attenuation, purely bound surface wave
4 - 5	radiation
5 - 6	non-spectral (improper) space harmonics

Similar effects occur when other space harmonics couple, or when a space harmonic couples with the plane wave skimming along the structure with free space velocity [19]. A typical dispersion plot for a periodic loaded structure is shown in figure 2.4. An overview of all special points is given in table 2.1

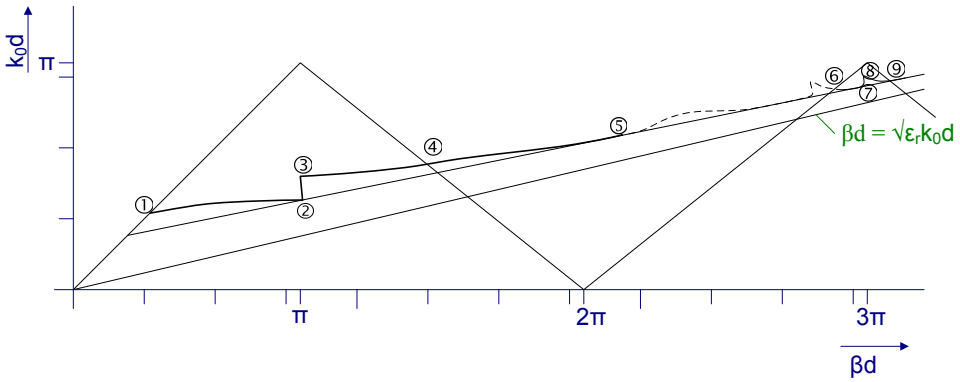

Figure 2.4: typical Brillouin diagram

2.4 Basic equations

The characteristic propagation behaviour of periodic open waveguides can be explained conveniently by using a k-β diagram, also called a dispersion plot. ([6] [15] and [17]) This dispersion plot is a graphical representation of the dispersion relation. To arrive at this dispersion relation we start with the basic Maxwell equations for a lossless configuration ($\sigma = 0$) in the space-frequency domain. As the electromagnetic field is transient (i.e it is causally related to the action of a source) we can apply the Laplace transformation with respect to the time coordinate. Following [7] we find, replacing s by $j\omega$ in case of steady-state analysis, that:

$$\begin{aligned} \partial_1\partial_1\hat{E}_2 + \partial_3\partial_3\hat{E}_2 + \omega^2\epsilon^{(i)}\mu^{(i)}\hat{E}_2 &= j\omega\mu^{(i)}\hat{J}_2^{ext} \\ \hat{H}_1 &= (j\omega\mu^{(i)})^{-1}\partial_3\hat{E}_2 \\ \hat{H}_3 &= -(j\omega\mu^{(i)})^{-1}\partial_1\hat{E}_2 \end{aligned} \tag{2.4}$$

As we will see later it is convenient (for numerical computations) to express our equations in normalized dimensionless quantities. For the structure shown in figure 2.1 a logical choice for the characteristic length is d and for the characteristic time $t_0 = \frac{d}{c_0} = d\sqrt{\epsilon_0\mu_0}$. Following the analysis described in appendix A, equation 2.4 becomes, after dropping all the accents:

$$\begin{aligned} \partial_1\partial_1\hat{e}_2 + \partial_3\partial_3\hat{e}_2 + \omega^2\epsilon_r^{(i)}\mu_r^{(i)}\hat{e}_2 &= j\omega\mu_r^{(i)}\hat{j}_2^{ext} \\ \hat{h}_1 &= (j\omega\mu_r^{(i)})^{-1}\partial_3\hat{e}_2 \\ \hat{h}_3 &= -(j\omega\mu_r^{(i)})^{-1}\partial_1\hat{e}_2 \end{aligned} \tag{2.5}$$

All three equations of system 2.5 are dimensionless. In the following analysis all measures of distance and time are assumed to be dimensionless. Table B.1 in appendix B gives an overview of the dimensional and the corresponding non-dimensional quantities.

After we divide the total set of x_3-coordinates in a set $\mathbb{S}$ of x_3-coordinates on the strip and a set $\mathbb{A}$ of x_3-coordinates in the aperture,

$$\begin{aligned} \mathbb{S} &= \left\{ N - \left(\frac{1-a}{2}\right) < x_3 < N + \left(\frac{1-a}{2}\right) \right\}, \qquad N \in \mathbb{Z} \\ \mathbb{A} &= \left\{ N + \left(\frac{1-a}{2}\right) \leq x_3 \leq (N+1) - \left(\frac{1-a}{2}\right) \right\}, \qquad N \in \mathbb{Z} \end{aligned}$$

we can write for the boundary conditions:

$$\begin{aligned} \hat{e}_2^{(0)}(-h, x_3) &= 0 \qquad && \forall\, x_3 \\ \hat{e}_2^{(0)}(0, x_3) - \hat{e}_2^{(1)}(0, x_3) &= 0 \qquad && \forall\, x_3 \\ \hat{h}_3^{(0)}(0, x_3) - \hat{h}_3^{(1)}(0, x_3) &= \begin{cases} 0 & x_3 \in \mathbb{A} \\ -\hat{j}_2 & x_3 \in \mathbb{S} \end{cases} \end{aligned} \tag{2.6}$$

The superscripts in equation 2.6 and all following equations refer to the region. E.g. $\epsilon_r^{(0)}$ refers to the permittivity of the dielectric. As the structure is periodic in the x_3-direction we can represent the modes propagating in this structure by their Floquet series ([14]):

$$\hat{e}_2^{(i)}(x_1, x_3) = \sum_{n=-\infty}^{\infty} \hat{e}_n^{(i)}(x_1) e^{-j(k_{30}+2\pi n)x_3} \tag{2.7}$$

in which every term represents a space harmonic. Following [20] and substitution of equation 2.7 into the first equation of 2.5 gives for a source-free domain:

$$\sum_{n=-\infty}^{\infty} \left\{ \partial_1\partial_1\hat{e}_n^{(i)}(x_1) + \left[\omega^2\epsilon_r^{(i)}\mu_r - k_{3n}^2\right] \hat{e}_n^{(i)}(x_1) \right\} e^{-jk_{3,n}x_3} = 0 \tag{2.8}$$

with

$$k_{3n} = k_{30} + 2\pi n \tag{2.9}$$

As this equation holds for all x_3 it must hold termwise. The system thus reduces to the second-order partial differential equation:

$$\partial_1 \partial_1 \hat{e}_n^{(i)}(x_1) + \left[\omega^2 \epsilon_r^{(i)} \mu_r - k_{3n}^2\right] \hat{e}_n^{(i)}(x_1) = 0 \tag{2.10}$$

The general solution for equation 2.10 is given by:

$$\begin{aligned} \hat{e}_n^{(i)}(x_1) &= A_n^{(i)} e^{jk_{1n}^{(i)} x_1} + B_n^{(i)} e^{-jk_{1n}^{(i)} x_1} \quad \text{with} & (2.11)\\ k_{1n}^{(i)} &= (\omega^2 \epsilon_r^{(i)} \mu_r - k_{3n}^2)^{\frac{1}{2}} & (2.12) \end{aligned}$$

The coefficients $A_n^{(i)}$ and $B_n^{(i)}$ are determined by the boundary conditions. On physical grounds we notice that for $|x_1| \to \infty$, $E_2^{(1)}$ does vanish for all x_3 (and so does $e_2^{(1)}$). As $k_{1,n}^{(1)}$ is chosen such that $Im\left\{k_{1,n}^{(1)}\right\} \leq 0$, equation 2.11 leads to $A_n^{(1)} = 0$ (radiation condition).

Substitution of equation 2.7 in equation 2.6 gives:

$$\begin{aligned} \sum_{n=-\infty}^{\infty} \hat{e}_n^{(0)}(-h) e^{-jk_{3n}x_3} &= 0 \qquad \forall\, x_3 \\ \sum_{n=-\infty}^{\infty} \left\{\hat{e}_n^{(0)}(0) - \hat{e}_n^{(1)}(0)\right\} e^{-jk_{3n}x_3} &= 0 \qquad \forall\, x_3 \qquad (2.13)\\ \sum_{n=-\infty}^{\infty} \left\{ \frac{\partial_1 \hat{e}_n^{(1)}(0)}{j\omega\mu_r^{(1)}} - \frac{\partial_1 \hat{e}_n^{(0)}(0)}{j\omega\mu_r^{(0)}} \right\} e^{-jk_{3n}x_3} &= \begin{cases} 0 & x_3 \in \mathbb{A} \\ -\hat{j}_2 & x_3 \in \mathbb{S} \end{cases} \end{aligned}$$

In view of equation 2.11 equation 2.13 becomes:

$$\begin{aligned} \sum_{n=-\infty}^{\infty} \left[A_n^{(0)} e^{-jk_{1n}^{(0)}h} + B_n^{(0)} e^{+jk_{1n}^{(0)}h}\right] e^{-jk_{3n}x_3} &= 0 \qquad \forall\, x_3 \\ \sum_{n=-\infty}^{\infty} \left[A_n^{(0)} + B_n^{(0)} - B_n^{(1)}\right] e^{-jk_{3n}x_3} &= 0 \qquad \forall\, x_3 \qquad (2.14)\\ \sum_{n=-\infty}^{\infty} \left[\frac{k_{1n}^{(0)}}{\omega\mu^{(0)}} A_n^{(0)} - \frac{k_{1n}^{(0)}}{\omega\mu^{(0)}} B_n^{(0)} + \frac{k_{1n}^{(1)}}{\omega\mu^{(1)}} B_n^{(1)} \right] e^{-jk_{3n}x_3} &= \begin{cases} 0 & x_3 \in \mathbb{A} \\ -\hat{j}_2 & x_3 \in \mathbb{S} \end{cases} \end{aligned}$$

Again, the first two sub-equations of equation 2.14 hold for all x_3, so there is term-wise equality, and consequently we can write:

$$\begin{aligned} B_n^{(0)} &= -A_n^{(0)} e^{-2jk_{1n}^{(0)}h} \\ B_n^{(1)} &= A_n^{(0)} + B_n^{(0)} \end{aligned} \tag{2.15}$$

Using this we express the last sub-equation of 2.14 in terms of $A_n^{(0)}$ only:

$$\sum_{n=-\infty}^{\infty} A_n^{(0)} \left\{ \left[1 + e^{-2jk_{1n}^{(0)}h}\right] \frac{k_{1n}^{(0)}}{\omega\mu_r^{(0)}} + \left[1 - e^{-2jk_{1n}^{(0)}h}\right] \frac{k_{1n}^{(1)}}{\omega\mu_r^{(1)}} \right\} \cdot e^{-jk_{3n}x_3} = \begin{cases} 0 & x_3 \in \mathbb{A} \\ -\hat{j}_2 & x_3 \in \mathbb{S} \end{cases} \tag{2.16}$$

Finally, as the dielectric slab is covered by metallic strips one more set of boundary conditions is prescibed.

$$\begin{aligned} \hat{e}_2^{(0)}(0, x_3) - \hat{e}_2^{(1)}(0, x_3) &= 0 \qquad x_3 \in \mathbb{A} \\ \hat{e}_2^{(0)}(0, x_3) = \hat{e}_2^{(1)}(0, x_3) &= 0 \qquad x_3 \in \mathbb{S} \end{aligned} \tag{2.17}$$

Combining this with equation 2.7 and 2.11 the two equations of 2.17 become

$$\sum_{n=-\infty}^{\infty} \left[A_n^{(0)} + B_n^{(0)}\right] e^{-jk_{3n}x_3} = \begin{cases} \hat{e}_2^{(1)} & x_3 \in \mathbb{A} \\ 0 & x_3 \in \mathbb{S} \end{cases} \tag{2.18}$$

again, we can express this in terms of $A_n^{(0)}$ only, using equation 2.15. This gives

$$\sum_{n=-\infty}^{\infty} A_n^{(0)} \left[1 - e^{-2jk_{1n}^{(0)}h}\right] e^{-jk_{3n}x_3} = \begin{cases} \hat{e}_2^{(1)} & x_3 \in \mathbb{A} \\ 0 & x_3 \in \mathbb{S} \end{cases} \tag{2.19}$$

2.5 Numerical Solution

Equation 2.16 is a description of the current $\hat{j}_2$ and equation 2.19 is a description of the $\hat{e}_2$-component of the electric field. Now taking the part of these two equations for which the right hand side of the equation is zero and looking at $2M + 1$ different (discrete) values of $x_{3m} \in \mathbb{A} \cup \mathbb{S}$, with $N = 0$

(that is the strip and aperture (one period) adjacent to the x_1-axis) we can write:

$$\bar{K}(k_{30})\,\bar{A} = \begin{bmatrix} k_{-M-M} & \dots & k_{-MM} \\ \vdots & \ddots & \vdots \\ k_{M-M} & \dots & k_{MM} \end{bmatrix} \begin{bmatrix} A_{-M}^{(0)} \\ \vdots \\ A_{M}^{(0)} \end{bmatrix} = 0 \tag{2.20}$$

where:

$$k_{mn} = \left\{ \left[1 + e^{-2jk_{1n}^{(0)}h}\right] \frac{k_{1n}^{(0)}}{\omega\mu_r^{(0)}} + \left[1 - e^{-2jk_{1n}^{(0)}h}\right] \frac{k_{1n}^{(1)}}{\omega\mu_r^{(1)}} \right\} e^{-jk_{3n}x_{3m}} \quad x_3 \in \mathbb{A}$$

and

$$k_{mn} = \left\{ \left[1 - e^{-2jk_{1n}^{(0)}h}\right] e^{-jk_{3n}x_3} \right\} \quad x_3 \in \mathbb{S} \tag{2.21}$$

Equation 2.20 is a system of $2M+1$ equations for $2M+1$ different complex values of $k_{3,n}$. For this system to have a solution (besides the trivial one) we need:

$$\det(K(Re\{k_{30}\}, Im\{k_{30}\})) = \begin{vmatrix} k_{-M-M} & \dots & k_{-MM} \\ \vdots & \ddots & \vdots \\ k_{M-M} & \dots & k_{MM} \end{vmatrix} = 0 \tag{2.22}$$

Equation 2.22 is a two dimensional zero-finding problem which can be solved numerically by efficient root-finding procedures. Most of the root-finding procedures assume that all components of k_{30} and $det(K(k_{30}))$ are of order unity. Although we normalized all our equations, one further improvement can be made. We write for equation 2.16:

$$\sum_{n=-\infty}^{\infty} \tilde{A}_n^{(0)} \left\{ \left[1 + e^{-2jk_{1n}^{(0)}h}\right] \left[1 - \frac{k_{3n}^2}{\omega^2\epsilon_r^{(0)}\mu_r^{(0)}}\right]^{\frac{1}{2}} + \left[1 - e^{-2jk_{1n}^{(0)}h}\right] \left[1 - \frac{k_{3n}^2}{\omega^2\epsilon_r^{(1)}\mu_r^{(1)}}\right]^{\frac{1}{2}} \left[\frac{\epsilon_r^{(1)}\mu_r^{(0)}}{\epsilon_r^{(0)}\mu_r^{(1)}}\right]^{\frac{1}{2}} \right\} \cdot e^{-jk_{3n}x_3} = \begin{cases} 0 & x_3 \in \mathbb{A} \\ -\hat{j}_2 & x_3 \in \mathbb{S} \end{cases} \tag{2.23}$$

If no real zero can be found for a given ω this indicates a stopband, sometimes also called an incomplete band gap, a region for which all propagating modes are damped, that is k_{30} is no longer purely real. When k_{30} has been

found by solving equation 2.22 we can determine the vector A as it is the null space of K.

Similar to equation 2.20 we write again:

$$\bar{K}(k_{30})\,\bar{A} = \begin{bmatrix} k_{-M-M} & \dots & k_{-MM} \\ \vdots & \ddots & \vdots \\ k_{M-M} & \dots & k_{MM} \end{bmatrix} \begin{bmatrix} \tilde{A}_{-M}^{(0)} \\ \vdots \\ \tilde{A}_{M}^{(0)} \end{bmatrix} = 0 \tag{2.24}$$

in which:

$$\tilde{A}_n^{(0)} = A_n^{(0)} \omega \left(\frac{\epsilon_r^{(0)}}{\mu_r^{(0)}} \right)^{\frac{1}{2}} \qquad x_3 \in \mathbb{A} \tag{2.25}$$

This gives for $x \in \mathbb{A}$:

$$\begin{aligned} k_{mn} = \Bigg\{ & \left[1 + e^{-2jk_{1n}^{(0)}h} \right] \left[1 - \frac{k_{3n}^2}{\omega^2 \epsilon_r^{(0)} \mu_r^{(0)}} \right]^{\frac{1}{2}} \\ & + \left[1 - e^{-2jk_{1n}^{(0)}h} \right] \left[1 - \frac{k_{3n}^2}{\omega^2 \epsilon_r^{(1)} \mu_r^{(1)}} \right]^{\frac{1}{2}} \left[\frac{\epsilon_r^{(1)} \mu_r^{(0)}}{\epsilon_r^{(0)} \mu_r^{(1)}} \right]^{\frac{1}{2}} \Bigg\} \cdot e^{-jk_{3n}x_3} \end{aligned} \tag{2.26}$$

The expressions for k_{mn} and for $\tilde{A}_n^{(0)} = A_n^{(0)}$ for $x \in \mathbb{S}$ remain unchanged. Equation 2.22, where the elements k_{nm} are given by equation 2.21 and 2.26 is the sought-after dispersion relation.

2.6 Used nomenclature in literature

In literature one finds several terms (with the same meaning) for E-mode and H-mode waves. The table below gives an overview of the different terms

Table 2.2: 2-D Wave Types

non-zero components	
$\{H_1, E_2, H_3\}$	$\{E_1, H_2, E_3\}$
nomenclature	
Transverse (TE) Electric Field	Transverse (TM) Magnetic Field
Perpendicular polarization	Parallel polarization
E-polarization	H-polarization
H-mode	E-mode

Chapter Three

Results

3.1 Introduction

Solving the determinantal equation has been done numerically, using the Fortran 90 programming environment. Initially a globally convergent Newton-Raphson routine called `newt()` from [13] was chosen. The determinant is calculated using the LU-decomposition routine `ludcmp()` from the same reference. It is noted that this routine has been rewritten to a routine capable of handling double precision complex variables.

As our determinant has to become zero and some of the variables are complex valued, this means that the real and imaginary part of the determinant must become zero. This is the case when the modulus of the determinant is zero. As taking the modulus is not an analytical operation, it seems wise to take the modulus squared as function value.

The `newt()` routine gave reasonable results when trying to find the roots of the determinantal equation and plotting these results in a dispersion plot. However, the written software was fragile and very sensitive to parameter changes. It appears that the `newt()` root-finding method (using a numerical calculated Jacobian) fails as the root is also a minimum.

A more feasible way is minimization of our determinant. Several minimization routines are available. A first choice was the 'Downhill Simplex Method in Multi-dimensions', which was chosen for two reasons. One, it only requires function evaluations and not derivatives. Two, it is described as a method that will 'get something working quickly'. It might not be the fastest method, but as the computational burden of our problem appears not to be too big, this acceptable.

The software was adapted for the use of the minimization routine `amoeba()`, again from [13]. Also the the routine `powell()`, from the same reference has

been implemented. Both minimization routines gave unsatisfactory results. All the aforementioned minimization routines were lacking the sophistication needed for the problem at hand. This sophistication was found in algorithm 365 described by Bach in [4]. Figure 3.1 gives an impression of the intelligence needed by the minimization routine to find the correct minimum and to follow it in the right valley.

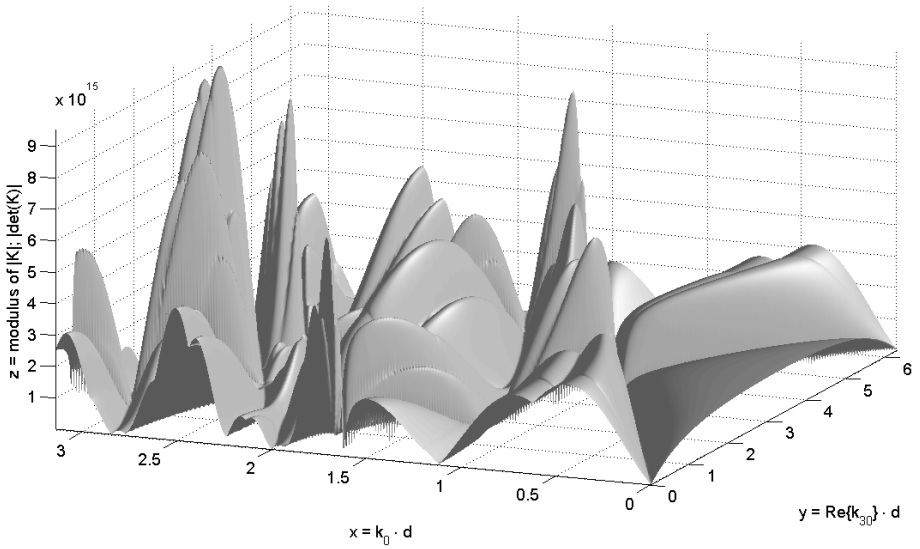

Figure 3.1: 3-D plot of the magnitude of the determinant in the k_{30}-k_0 plane, $Im\{k_{30}\} = 0$

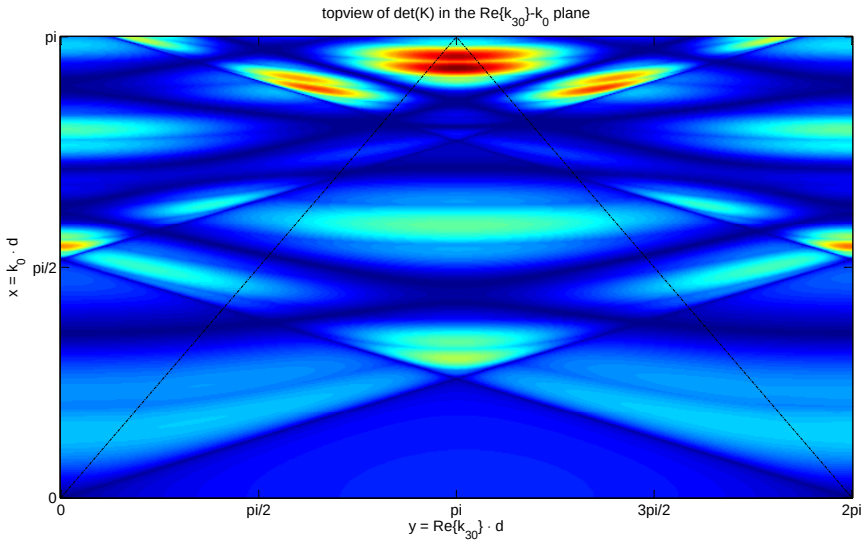

Figure 3.2: 2-D topview of figure 3.1

A top view of figure 3.1 is shown in figure 3.2. This figure clearly shows the dispersion curves of the unloaded structure for the basic space harmonic as dark lines starting from the origin and $n = -1$ space harmonic starting from 2π. Closer inspection reveals even the effect of the branch-cuts, here emphasized with black lines from $(0, 0)$ and $(2\pi, 0)$ to (π, π).

In this section we present the results of four different types of numerical experiments. The numerical parameter values for the different experiments are listed in table C.1 of appendix C. In the first experiment we have investigated the influence of the number of space harmonics taken along in our calculations. The second experiment involved variation of the permittivity of the dielectric and in the third experiment the slot size was varied. In the last experiment the influence of the height (h) of the dielectric was analysed. In all experiments a small imaginary part for ω (or $\epsilon_r^{(i)}$) was introduced, which gave a spectacular improvement of the numerical behaviour.

3.1.1 Variation of number of space harmonics

The number of space harmonics determines how exact the real electric field is approximated. Beside that, it also determines the number of x_3-points used in the discretization. To be able to analyse influence of the number of space harmonics all other parameters were chosen constant. A logical choice is to choose the slot size equal to the strip size, $a = 0.5$.

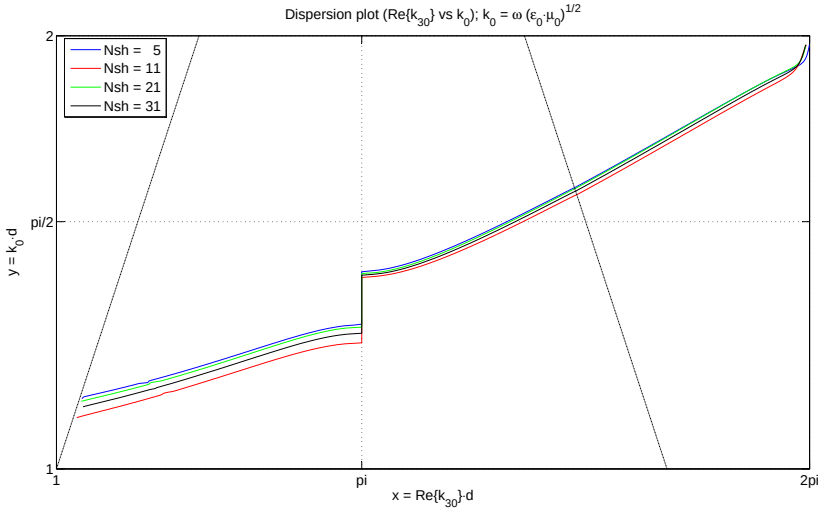

Figure 3.3: Influence of variation of number of space harmonics (Nsh) on $Re\{k_{30}\}$

We take $\epsilon_r^{(0)} = 15$ and $h = 0.667$. This places the dispersion curve nicely in the middle of the triangle and h is not an integral multiple of a. Figure 3.3 shows the dependency of the $Re\{k_{30}\} - k_0$ plot on the number of space harmonics. The first thing that was noticed, when increasing the number of space harmonics, is the increase of computational burden. This however, was not an issue as all computations for one single dispersion curve were completed within one minute. As for all other parameters, variation of the number of space harmonics gave need to vary the starting frequency, from which our dispersion curve start, as well. This starting frequency needs to be chosen such, that we start in the 'right valley'.

The dispersion curves shown in figure 3.3 nicely show the structure, as described at the end of paragraph 2.3, including stopband and cut-off frequency. The graph oscillates in the direction of the real solution. I.e. the $Nsh = 31$ curve is in between the $Nsh = 21$ and $Nsh = 11$ curve.

This last behaviour is also noticed in figure 3.4. This figure shows the attenuation coefficient $Im\{k_{30}\}$ versus k_0. The expected increase of the $Im\{k_{30}\}$ is found in the stopband (the first peak) and when the dispersion curve enters the FWR (the second peak). This latter happens when the dispersion curve just emerges from the slow-wave triangle. In both cases the increase of the attenuation coefficient indicates radiation travelling away from the structure.

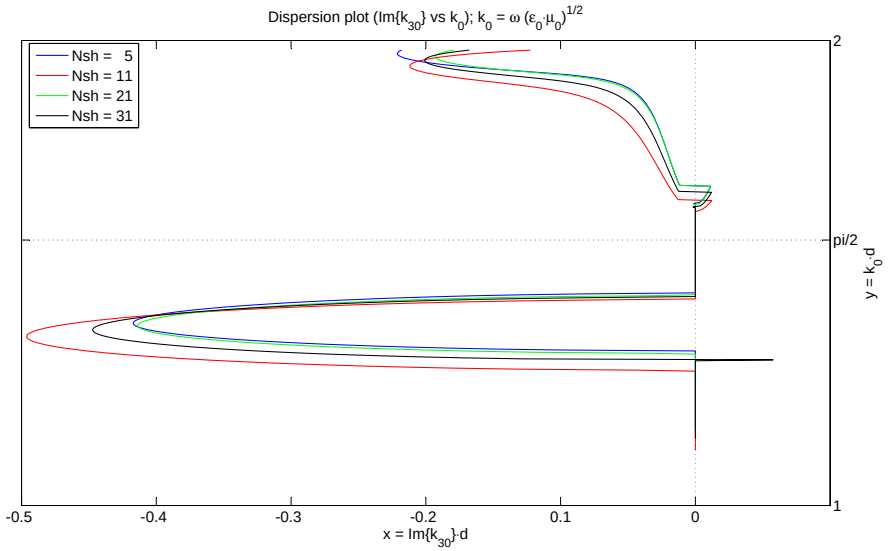

Figure 3.4: Influence of variation of number of space harmonics (Nsh) on $Im\{k_{30}\}$

3.1.2 Variation of permittivity of the dielectric

The second experiment was to analyse the dependency of the dispersion on the permittivity of the dielectric, $\epsilon_r^{(0)}$. Figure 3.5 shows the dispersion curves for $\epsilon_r^{(0)} = 15.0$ (the default) and $\epsilon_r^{(0)} = 4.0$.

To study the influence of $\epsilon_r^{(0)}$, we set all other parameters to their default values. Looking at figure 3.5 we notice three things, when lowering $\epsilon_r^{(0)}$. First the cut-off frequency raises, second the stop-band becomes larger and last the slope of the curve, which corresponds with the group-velocity $v_g = \partial_\omega / \partial k_{30}$, increases.

The wavespeed in the dielectric increases, when the permittivity is decreased. For the wavelength to *fit* the dimensions of the structure a higher frequency is required.

Decreasing the permittivity causes an increase of slope of the dispersion curve. This causes more shallow valleys for the determinantal equation, giving an increase of the width of the stop-band. It could even be suggested that the square of the ratio of the two stop-bands is the ratio of the two different values of permittivity.

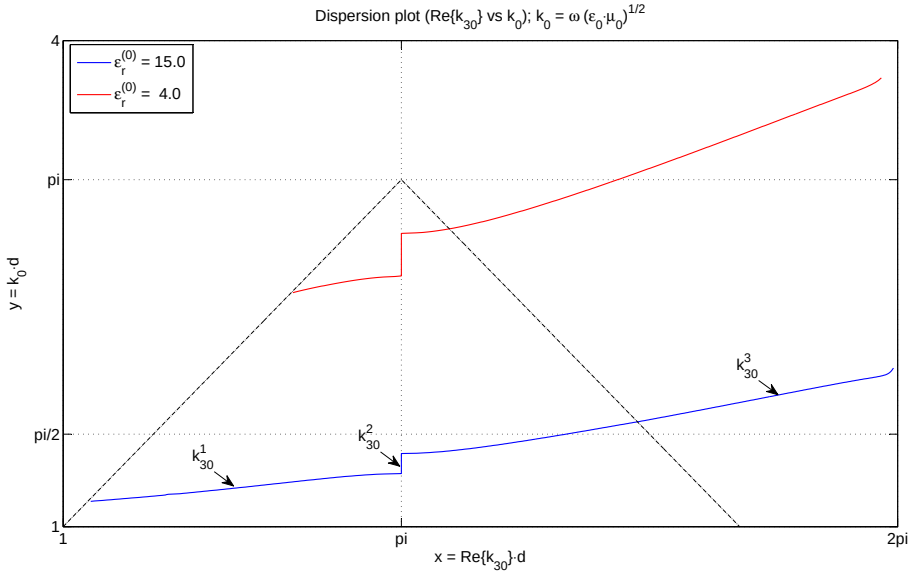

Figure 3.5: Influence of variation of permittivity of the dielectric on $Re\{k_{30}\}$

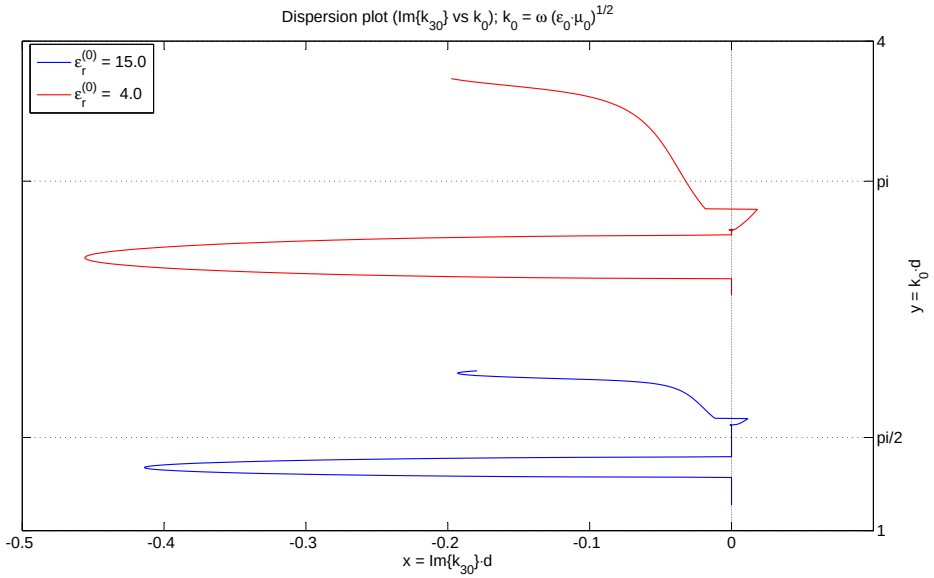

Figure 3.6: Influence of variation of permittivity of the dielectric on $Im\{k_{30}\}$

The increase of the slope, or group-velocity is a direct consequence of the change of permittivity. This can be seen as follows. The phase-velocity increases, when the permittivity decreases and the group-velocity is proportionally related to the phase-velocity. Figure 3.6 shows an increase of the $Im\{k_{30}\}$ as can be expected with a wider stop-band.

3.1.3 Variation of slot dimensions

The most important parameter in the periodic structure is the strip size (or slot dimension). As we did not make any assumptions about strips being wide of narrow our method can be applied to both structures. Figure 3.7 shows the dispersion diagrams for aperture sizes of 10, 50 and 90 percent of the periodic distance d.

Looking at the three different dispersion curves in figure 3.7 we observe with decreasing aperture size an increase of the cut-off frequency, and a decrease of the width of the stop band. For a small aperture we look at the limiting case of a closed waveguide. This type of waveguide is known to have a cut-off frequency, and no stop band. The other limiting case, the open waveguide does not have a cut-off frequency. The increase of cut-off frequency for decreasing aperture size is in agreement with this.

The increase of the width of the stop band can be explained similarly as in the second last paragraph of section 3.1.2. Figure 3.8 visualises the intensity and vanishing of the stop band clearly.

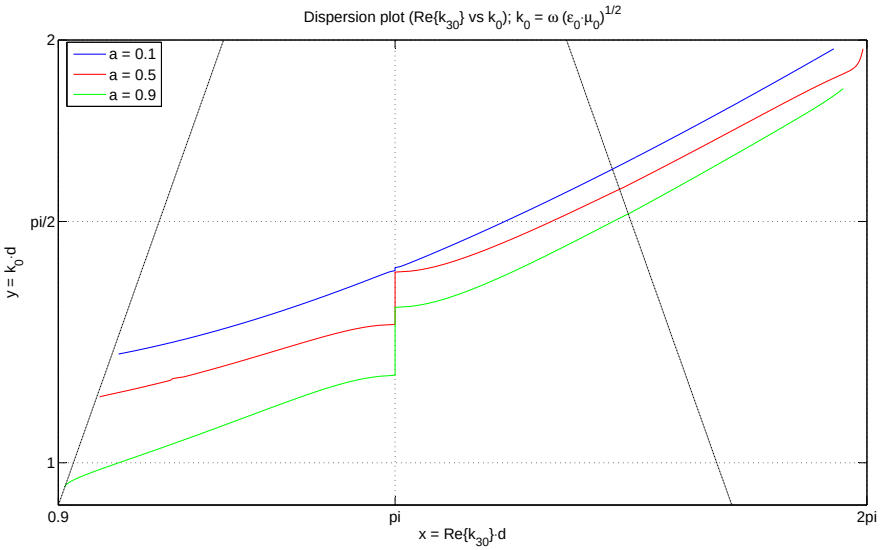

Figure 3.7: Influence of variation of slot dimensions on $Re\{k_{30}\}$

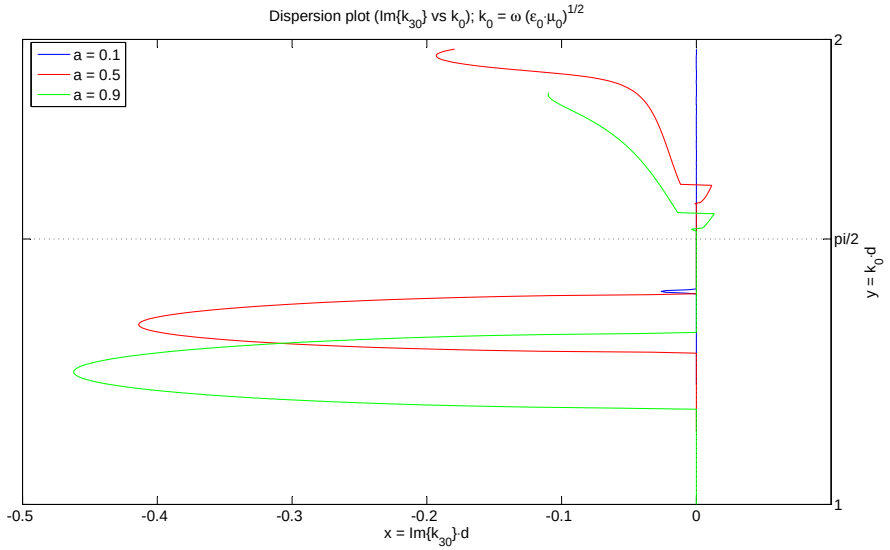

Figure 3.8: Influence of variation of slot dimensions on $Im\{k_{30}\}$

3.1.4 Variation of height of the dielectric

The last parameter of the structure that we vary is the height of the dielectric layer. The dispersion curves for three different heights are shown in figure 3.9.

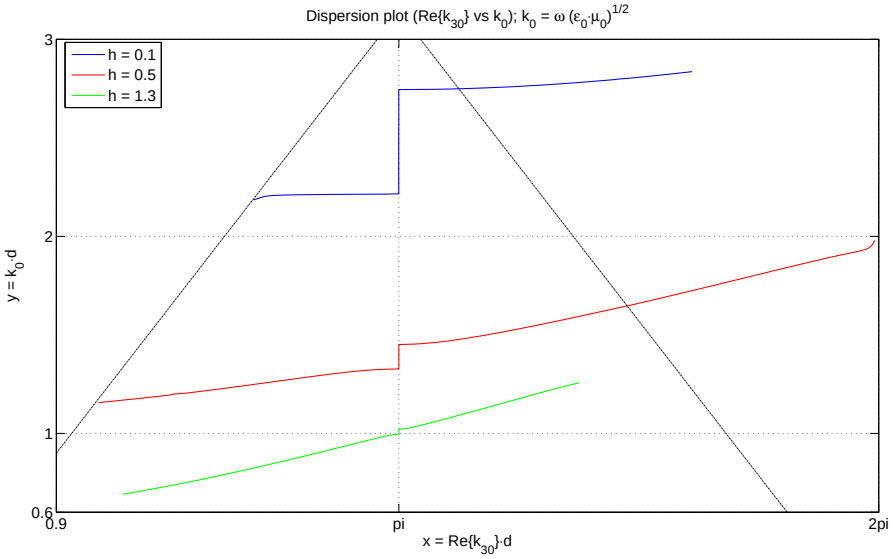

Figure 3.9: Influence of height of the dielectric on $Re\{k_{30}\}$

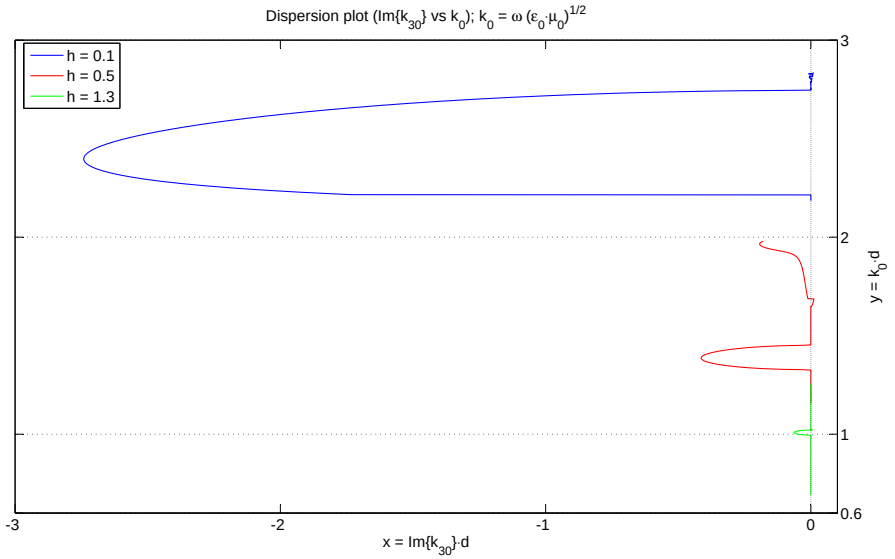

Figure 3.10: Influence of height of the dielectric on $Im\{k_{30}\}$

We see that below a certain height the stop band expands heavily, as does the attenuation (see figure 3.10). Note the change in scale with respect to the previous figures of $Im\{k_{30}\}$. From the shape and position of the dispersion curve we can conclude that almost no frequency propagates. For increasing height of the layer we see that the dispersion curve approaches the dispersion curve of an unloaded structure, as for increasing height the effect of the loading slowly vanishes.

3.2 Visualisation of the electric field

In this final section we will show three visualisations of the x_2-component of the electric field and one of the current density. To be able to calculate these quantities we first need to calculate the vector A containing all the coefficients for all the space harmonics. As the $K-$matrix is now known this is rather simple. We have calculated the vector A, using again the (complex) routine `ludcmp()`, now followed by a (complex) LU-backsubstitution routine `lubksb()`, again from [13]. The LU-decomposition results in:

$$\bar{K}\ \bar{A} = L\ U\ \bar{A} = P\ b \tag{3.1}$$

in which P is a row-permutation matrix. As $b = 0$ we can write:

$$L\ U\ \bar{A} = 0 \tag{3.2}$$

Defining

$$y = U\ \bar{A} \tag{3.3}$$

we rewrite equation 3.2 as

$$L\ y = 0 \tag{3.4}$$

which leads to $y = 0$ as L contains no rows only containing zeros. Knowing this we can write equation 3.2 as

$$U\ \bar{A} = 0 \tag{3.5}$$

Close inspection of the matrix U has shown that the pivot β_{nn} in last row of U is (nearly) zero. This means that we can set the element A_n of $\bar{A}$ to any value. A logical choice is $A_n = 1$. Knowing A_n, all the other n-1 components of $\bar{A}$ can now be calculated.

Now all the variables are known, we can calculate the x_2-component of the electric field using equation 2.7. Multiplying this with $e^{j\omega t}$ and taking the real part of the result, we can visualise the electric field in the space-time domain. Figure 3.11 shows E_2 for a randomly chosen frequency that is located on the default dispersion curve e.g. as shown in figure 3.5 where k_{30} is located before the stop band ($k_{30} = k_{30}^1$).

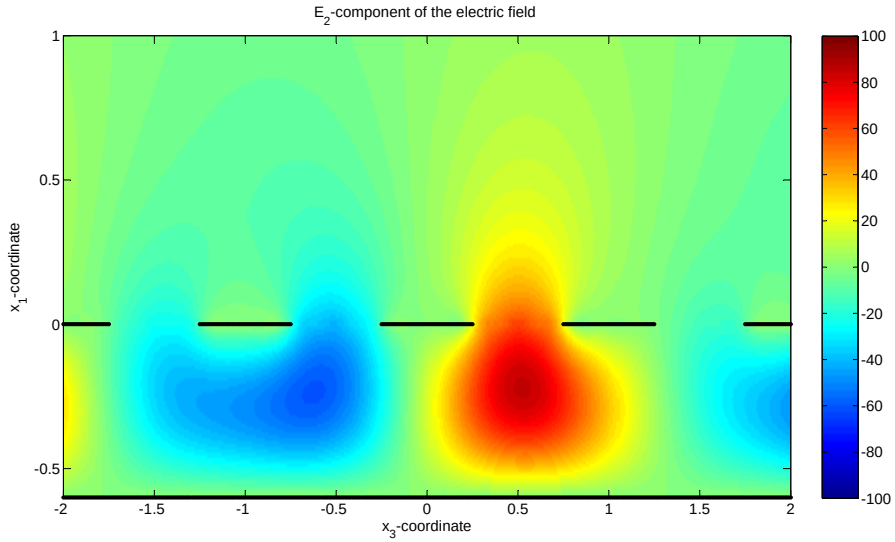

Figure 3.11: Visualisation of E_2 for $k_{30} < k_{30}^{stopband}$

The figure above shows clearly the surface waves or propagating modes in the structure. Plotting figure 3.11 when time passes, as a kind of movie, we see the maxima (and minima) of the waves are propagating from left to right.

Figure 3.12 shows the distribution of the electric field component E_2 for a k_{30} such that the frequency is in the middle of the vertical jump of the default dispersion curve ($k_{30} = k_{30}^2$ in figure 3.5). We notice the increase of radiation, as $Im\{k_{30}\} \neq 0$ and the increase of frequency which is clear from the increase of the number of periods between the plates. In this stop band we see the expected non-propagation behaviour. The maxima and minima do not propagate but change of polarity continuously.

When the dispersion curve emerges from the slow wave triangle the corresponding mode becomes a fast wave and starts to be radiated. Picking $(k_{30}, \omega) \in$ FWR ($k_{30} = k_{30}^3$ in figure 3.5) and visualising the E_2-component electric field results in figure 3.13. Again the increase of frequency is clearly visible. The figure also shows the electric field radiating away from the

structure with a certain angle with respect to broadside. In this case, again, the waves are propagating from left to right.

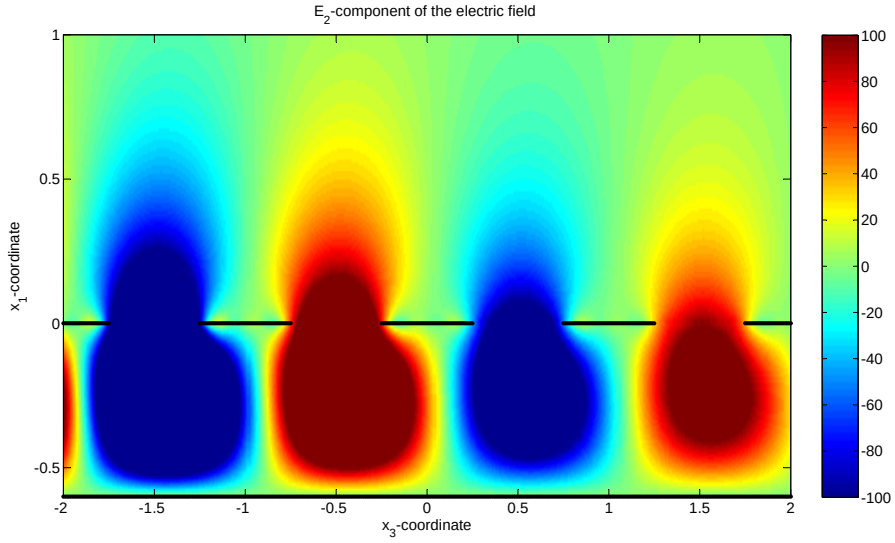

Figure 3.12: Visualisation of E_2 for $k_{30} = k_{30}^{stopband}$

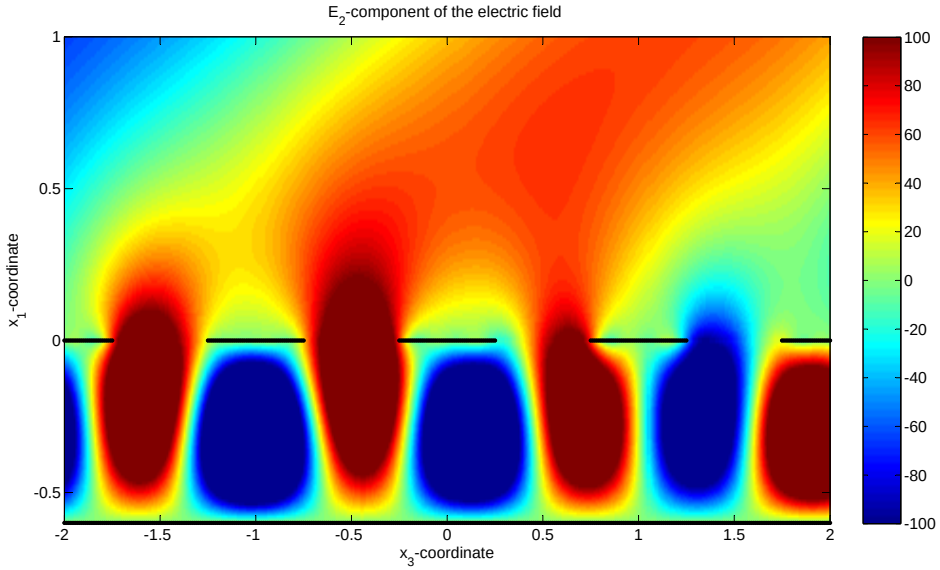

Figure 3.13: Visualisation of E_2 for $(k_{30}, \omega) \in$ FWR

In the last figure of this section we show the distribution of the current density J_2 along the width of the strip. The red crosses indicate the discrete

values of x_{3m} as introduced in equation 2.20. The figure shows clearly that an assumption of a sinusoidal current distribution over the strip is incorrect.

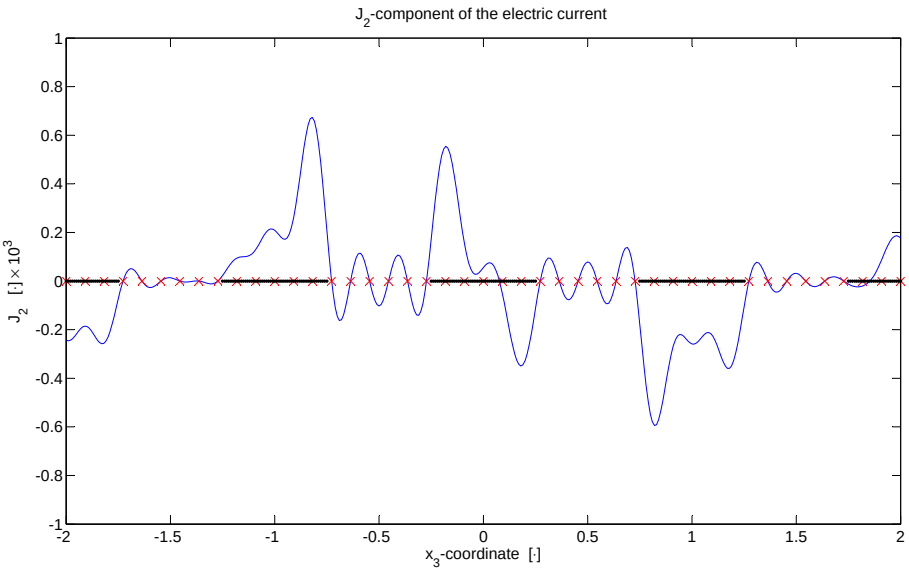

Figure 3.14: Visualisation of J_2 for $k_{30} < k_{30}^{stopband}$

3.3 Discussion of the results

In this chapter we have demonstrated that the solutions of the determinantal equation for a periodically loaded open waveguide structure, as we have derived it, correspond very well with existing theory, that has been proven by experiments. The analysis has been performed without making any assumptions about the strip dimensions.

In section 3.1.1 we have shown the influence of the number of space harmonics on the solution of the determinantal equation. It has been demonstrated that increasing the number of space harmonics improves the solution of the determinantal equation, after which the electric field can be approximated better.

In the following section 3.1.2 we analysed the effect of the variation of ϵ_r. We have demonstrated the effect of the variation of ϵ_r on the cut-off frequency and the width of the stop band. As $\epsilon_r = 15.0$ gave nicer numerical results we have continued using this ϵ_r as a default value.

Subsequently in section 3.1.3 we have discussed the variation of the slot size. It has been shown how the cut-off frequency and the width of the stop band vary for different slot sizes. Also an extension to the limiting case of slot size of zero and hundred percent have been discussed.

In the penultimate section 3.1.4 the variation of the height of the dielectric has been investigated. We have seen that an increase of the height of the dielectric in the limiting case results in the dispersion curve of a non-loaded structure.

Finally in section 3.2 we have shown some plots of the x_2-component of the electric field and the current density.

In our theoretical analysis all calculations have been done for a two-dimensional structure with infinite dimensions in the x_3-direction and that is invariant in the x_2-direction. For more practical applications the analysis needs to be expanded to finite dimensional structures in *three* dimensions. The analysis in this report is a very good start for this.

Chapter Four

Conclusion & recommendations

In this thesis we have shown a new method to solve Maxwell's equations for a two-dimensional periodically loaded open waveguide that is infinitely long in the lateral (x_3) direction and invariant in the transverse (x_2) direction. This method, contrary to existing methods, does not make any assumptions about the width of the strips loading the structure, nor about the current in those strips. Based on this research we can conclude/confirm that:

- The new method to solve Maxwell's equations without assumptions about width of and current in the strips is a good method to model the waveguide dispersion characteristics.
- The assumption that that current in the strips has a sinusoidal shape has been proven to be incorrect.
- An increase of the number of space harmonics, increases the accuracy of the found solution. The computational burden of the method is limited, even for a high numbers (> 80) of space harmonics
- For common values of ϵ_r, ($1 \leq \epsilon_r \leq 4$) the frequency band for which surface waves appear is rather limited.
- The change in dispersive properties of a periodically loaded open waveguide for slotwidths ranging from wide to narrow can be considered in a continuous way. In the limiting cases of slotwidths of zero or one-hundred percent of the periodic distance, the dispersive properties approach those of respectively closed/open waveguides.
- In case of increasing heights of the dielectric the influence of the loading vanishes.

The performed research gives reason for the following recommendation:

- The developed model for a 2-D periodically loaded open waveguide should be expanded to a 3-D model.

- This work could be extended to periodically fed antennas (such as patch arrays.

Appendix A

Normalization of Maxwell's equations

Maxwell's equations in a lossless medium are:

$$-\nabla \times \bar{H} + \epsilon \partial_t \bar{E} = -\bar{J}^{ext} \tag{A.1}$$
$$\nabla \times \bar{E} + \mu \partial_t \bar{H} = -\bar{K}^{ext} \tag{A.2}$$

Suppose that we want to express all spatial coordinates in terms of a characteristic length x_0, and the time coordinate in terms of a characteristic time t_0. Then we may define the normalized, dimensionless coordinates $\bar{x}'$ and t' as:

$$\bar{x}' = \frac{\bar{x}}{x_0} \tag{A.3}$$
$$t' = \frac{t}{t_0} \tag{A.4}$$

As a result of the transformation in equations A.3 and A.4 we find the transformed operators:

$$\nabla' = x_0 \nabla \tag{A.5}$$
$$\partial_{t'} = t_0 \partial_t \tag{A.6}$$

Further, the quantities $\bar{E}, \bar{H}, \bar{J}^{ext}$ and $\bar{K}^{ext}$ are transformed into $\bar{E}'$, $\bar{H}'$, $\bar{J}'^{ext}$ and $\bar{K}'^{ext}$.

$$\bar{E}(\bar{x}, t) = \bar{E}'(\bar{x}', t') \tag{A.7}$$
$$\bar{H}(\bar{x}, t) = \bar{H}'(\bar{x}', t') \tag{A.8}$$
$$\bar{J}^{ext}(\bar{x}, t) = \bar{J}'^{ext}(\bar{x}', t') \tag{A.9}$$
$$\bar{K}^{ext}(\bar{x}, t) = \bar{K}'^{ext}(\bar{x}', t') \tag{A.10}$$

In view of equations A.5 - A.10, equations A.1 and A.2 turn into:

$$-\nabla' \times \bar{H}' + \tfrac{x_0}{t_0} \epsilon \partial_{t'} \bar{E}' = -x_0 \bar{J}'^{ext} \tag{A.11}$$
$$\nabla' \times \bar{E}' + \tfrac{x_0}{t_0} \mu \partial_{t'} \bar{H}' = -x_0 \bar{K}'^{ext} \tag{A.12}$$

A particular choice is to take t_0 equal to the time required to travel a distance x_0, i.e.:

$$t_0 = \frac{x_0}{c} = x_0\sqrt{\epsilon\mu} \tag{A.13}$$

In that case, equations A.11 and A.12 become:

$$-\nabla' \times \bar{H}' + \sqrt{\frac{\epsilon}{\mu}}\partial_{t'}\bar{E}' = -x_0\bar{J}'^{ext} \tag{A.14}$$

$$\nabla' \times \bar{E}' + \sqrt{\frac{\mu}{\epsilon}}\partial_{t'}\bar{H}' = -x_0\bar{K}'^{ext} \tag{A.15}$$

Further, suppose that we want to express $\bar{E}'$ and $\bar{H}'$ in terms of a characteristic electric field strength E_0 and a characteristic magnetic field strength H_0. Then we may define the normalized, dimensionless quantities, $\bar{e}$ and $\bar{h}$ as:

$$\bar{e} = \frac{E'}{E_0} \tag{A.16}$$

$$\bar{h} = \frac{H'}{H_0} \tag{A.17}$$

In view of equations A.16 and A.17, equations A.14 and A.15 become:

$$-\nabla' \times \bar{h} + \frac{E_0}{H_0}\sqrt{\frac{\epsilon}{\mu}}\partial_{t'}\bar{e} = -\frac{x_0}{H_0}\bar{J}'^{ext} \tag{A.18}$$

$$\nabla' \times \bar{e} + \frac{H_0}{E_0}\sqrt{\frac{\mu}{\epsilon}}\partial_{t'}\bar{h} = -\frac{x_0}{E_0}\bar{K}'^{ext} \tag{A.19}$$

A particular choice is to take:

$$H_0 = YE_0 = \sqrt{\frac{\epsilon}{\mu}}E_0 \tag{A.20}$$

where Y is the plane wave admittance.

Using this, equations A.18 and A.19 become:

$$-\nabla' \times \bar{h} + \partial_{t'}\bar{e} = -\frac{x_0}{E_0}\sqrt{\frac{\mu}{\epsilon}}\bar{J}'^{ext} \tag{A.21}$$

$$\nabla' \times \bar{e} + \partial_{t'}\bar{h} = -\frac{x_0}{E_0}\bar{K}'^{ext} \tag{A.22}$$

If we now define the new quantities:

$$\bar{j}^{ext} = \frac{x_0}{E_0}\sqrt{\frac{\mu}{\epsilon}}\bar{J}'^{ext} \tag{A.23}$$

$$\bar{k}^{ext} = \frac{x_0}{E_0}\bar{K}'^{ext} \tag{A.24}$$

we finally may write equations A.21 and A.22 as:

$$-\nabla' \times \bar{h} + \partial_{t'}\bar{e} = -\bar{j}^{ext} \tag{A.25}$$

$$\nabla' \times \bar{e} + \partial_{t'}\bar{h} = -\bar{k}^{ext} \tag{A.26}$$

Note that all quantities in equations A.25 and A.26 are dimensionless.

In steady state analysis, we can replace $\partial_{t'}$ by $j\omega'$ and write equations A.25 and A.26 as:

$$-\nabla' \times \bar{h} + j\omega'\bar{e} = -\bar{j}^{ext} \tag{A.27}$$

$$\nabla' \times \bar{e} + j\omega'\bar{h} = -\bar{k}^{ext} \tag{A.28}$$

Since $\partial_t \rightarrow j\omega$ and $\partial_{t'} \rightarrow j\omega'$ and in view of equation A.6 we find that:

$$\omega' = t_0\omega \tag{A.29}$$

Note that ω' is also dimensionless.

Appendix B

Non dimensional quantities in Maxwell's equations

Table B.1: Non dimensional quantities in Maxwell's equations

Dimensional quantity	Dimension	Divisor	Non-dimensional quantity
x_1	[m]	d	$x_1' = \frac{x_1}{d}$
x_3	[m]	d	$x_3' = \frac{x_3}{d}$
∂x_1	$[\mathrm{m}]^{-1}$	$\frac{1}{d}$	$\partial x_1' = d \cdot \partial x_1$
∂x_3	$[\mathrm{m}]^{-1}$	$\frac{1}{d}$	$\partial x_3' = d \cdot \partial x_3$
a	[m]	d	$a' = \frac{a}{d}$
h	[m]	d	$h' = \frac{h}{d}$
$\hat{E}_2$	$[\mathrm{V{\cdot}m}]^{-1}$	E_0	$\hat{e}_2 = \frac{\hat{E}_2}{\hat{E}_0}$
$\hat{H}_1$	$[\mathrm{A{\cdot}m}]^{-1}$	$\sqrt{\frac{\epsilon_0}{\mu_0}} E_0$	$\hat{h}_1 = \frac{\hat{H}_1}{E_0} \sqrt{\frac{\mu_0}{\epsilon_0}}$
$\hat{H}_3$	$[\mathrm{A{\cdot}m}]^{-1}$	$\sqrt{\frac{\epsilon_0}{\mu_0}} E_0$	$\hat{h}_3 = \frac{\hat{H}_3}{E_0} \sqrt{\frac{\mu_0}{\epsilon_0}}$
ϵ	$[\mathrm{F{\cdot}m}]^{-1}$	ϵ_0	$\epsilon_r = \frac{\epsilon}{\epsilon_0}$
μ	$[\mathrm{H{\cdot}m}]^{-1}$	μ_0	$\mu_r = \frac{\mu}{\mu_0}$
$\hat{J}_2$	$[\mathrm{V{\cdot}m}]^{-2}$	$\frac{E_0 \sqrt{\frac{\epsilon_0}{\mu_0}}}{x_0}$	$\hat{j}_2 = \frac{\hat{J}_2}{E_0} x_0 \sqrt{\frac{\mu_0}{\epsilon_0}}$
ω	$[\mathrm{rad{\cdot}s}]^{-1}$	$\frac{c_0}{d}$	$\omega' = \frac{d}{c_0} \omega$
$k_{3,0}$	$[\mathrm{m}]^{-1}$	$\frac{1}{d}$	$k_{3,0}' = k_{3,0} \cdot d$

to facilitate writing, the quotes are dropped in the analysis in chapter 2

Appendix C

Numerical experiments parameter values

Table C.1: Numerical experiments parameter values

NUMERICAL EXPERIMENTS			
Experiment I			
a	b	c	d
Nsh = 5	**Nsh = 11**	**Nsh = 21**	**Nsh = 31**
ϵ_r = 15.0	ϵ_r = 15.0	ϵ_r = 15.0	ϵ_r = 15.0
a = 0.5	a = 0.5	a = 0.5	a = 0.5
h = 0.667	h = 0.667	h = 0.667	h = 0.667
freqMin = 0.185	freqMin = 0.178	freqMin = 0.184	freqMin = 0.182
freqMax = 0.315	freqMax = 0.315	freqMax = 0.315	freqMax = 0.315
Experiment II			
a	b		
Nsh = 21	Nsh = 21		
ϵ_r = 15.0	**ϵ_r = 4.0**		
a = 0.5	a = 0.5		
h = 0.667	h = 0.667		
freqMin = 0.184	freqMin = not noted		
freqMax = 0.315	freqMax = not noted		
Experiment III			
a	b	c	
Nsh = 21	Nsh = 21	Nsh = 21	
ϵ_r = 15.0	ϵ_r = 15.0	ϵ_r = 15.0	
a = 0.1	**a = 0.5**	**a = 0.9**	
h = 0.667	h = 0.667	h = 0.667	
freqMin = 0.2001	freqMin = 0.184	freqMin = 0.150	
freqMax = 0.315	freqMax = 0.415	freqMax = 0.300	
Experiment IV			
a	b	c	
Nsh = 21	Nsh = 21	Nsh = 21	
ϵ_r = 15.0	ϵ_r = 15.0	ϵ_r = 15.0	
a = 0.5	a = 0.5	a = 0.5	
h = 0.1	**h = 0.5**	**h = 1.3**	
freqMin = 0.34772	freqMin = 0.184	freqMin = 0.110	
freqMax = 0.45136	freqMax = 0.315	freqMax = 0.204	

Bibliography

[1] N.W. Ashcroft and N.D. Mermin. *Solid State Physics*. Saunders College, 1976.

[2] Paulotto S. Jackson D.R. Baccarelli, P. and A.A. Oliner. A new brillouin dispersion diagram for 1-d periodic printed structures. *Microwave Theory and Techniques, IEEE Transactions on, Vol. 55, No. 7 pp, 1484-1495*, Jul 2007.

[3] H. Bach. Algorithm 365 complex root finding [c5]. *Communications of the ACM Vol. 12 Iss. 12 pp. 686-687*, December 1969.

[4] H. Bach. On the downhill method. *Communications of the ACM Vol. 12 Iss. 12 pp. 675-677 684*, December 1969.

[5] J. van Badel. *Electromagnetic Fields*. Wiley Interscience, 2007.

[6] P. Balling. Periodically modulated dielectrically filled waveguide as a microwave antenna. *Electronic Letters Vol. 5 No. 21 pp. 508-510*, October 16, 1969.

[7] Blok H. Verweij M.D. Berg, P.M. van den. *Electromagnetic Waves, An Introductory Course*. DUP Blue Print, 2001.

[8] L. Brillouin. *Wave Propagation in Periodic Structures*. Dover Publications Inc., 2003.

[9] N.V. Budko. Electromagnetic radiation, scattering and imaging, 2004. Lecture notes for the course ET4356.

[10] C.M. Butler and K.R. Umashankar. Electromagnetic penetration through an aperture in an infinite, planar screen separating two half space of different electromagnetic properties. *Radio Science Vol. 11 Num. 7 pp. 611-619*, July 1976.

[11] R.E. Collin. *The Field Theory of Guided Waves*. IEEE Press, 2nd edition, 1991.

[12] V.N. Datsko and A.A. Kopylov. On surface electromagnetic waves. *PHYS-USP, Vol. 51 No. 1 pp. 101102.*, 2008.

[13] Press W.H. Teukolsky S.A. Flannery, B.P. and Vetterling W.T. *Numerical Recipes in Fortran 77.* Cambridge University Press, 2001.

[14] M.J. Gans. A general proof of floquets theorem. *IEEE transactions on microwave theory and techniques pp. 384-385*, May 1965.

[15] J. Jacobson. Analytical, numerical, and experimental investigation of guided waves on a periodically strip-loaded dielectric slab. *Antennas and Propagation, IEEE Transactions on, pp. 379-388*, May 3, 1970.

[16] H.A. Kalhor. Electromagnetic scattering by a dielectric slab loaded with a periodic array of strips over a ground plane. *Antennas and Propagation, IEEE Transactions on, Vol. 36 pp. 147-151*, January 1988.

[17] A.A. Oliner. Guided complex waves on slow-wave periodic structures. *Electromagnetic Wave Theory pt. 1*, 1967.

[18] Collin R.E. and Zucker F.J. *Antenna Theory part 1.* McGraw-Hill Book Company, 1969.

[19] Collin R.E. and Zucker F.J. *Antenna Theory part 2.* McGraw-Hill Book Company, 1969.

[20] R.A. Sigelmann. Surface waves on a grounded dielectric slab covered by a periodically slotted conducting plane. *Antennas and Propagation, IEEE Transactions on, Vol. 15 pp. 672-676*, September 1967.

[21] M.D. Verweij. Electromagnetic waveguides, 2006. Lecture notes for the course ET4356.

[22] H. Voss. A jacobidavidson method for nonlinear eigenproblems. *Computational Science - ICC2 2004, 4th International Conference Krakow Poland Proceedings Part II pp. 34-41*, June 2004.

[23] P. Yariv, A.. Yeh and C-S. Hong. Electromagnetic propagation in periodic stratified media. i. general theory. *J. Opt. Soc. Am. Vol. 67 No. 4 pp. 423-437*, 1977.

[24] F.J. Zucker. Theory and applications of surface waves. *Il Nuovo Cimento Vol. 9 Sup. 3*, March 1952.